Nonlinear Stress Analysis and Review for the Prestressed Concrete Reactor Vessel of the HTR500-Type

Tai-Jun Wang
Tsinghua University, Beijing, PRC
Jurgen Altes
Institute of Nuclear Safety Research, KEA, Juelich, FRG

ABSTRACT

Since 1982 design and research work has been started for the HTR500 Mwe plant as a potential follow-on project of the THTR300 in the FRG. The assignment of this paper is to review the stress analysis of the PCRV of the HTR500-type, which is required to get to know the entire behaviour of the concrete vessel under various conditions including the elastic, elasto-plastic, limit state and creep behaviour. (Wang, T. J., Altes, J., 1988)

Curved triangular, quadrilateral and membrane shell elements are used in the axisymmetrical finite element stress analysis. The incremental model in the form of tangential stress-strain law has been chosen as the constitutive model for the concrete. The numerical initial iteration method with constant stiffness is utilized. The creep strain is treated as a linear functional of the stress history and dependent on temperature, humidity and aging. The calculation of the creep behaviour is carried out up to 7 years using the models of SEKI et al (Seki, S. et al 1972) and WYLFA concrete (Browne, R. D., et al 1969). In the first model the influence of temperature, humidity and the interaction between them is fully considered. The computer code used for this analysis is called SMART (Argyris, J. H., et al 1982) and the post-processing code is called RAPS (Koschmieder, D., et al 1980).

Under the action of prestressing alone most parts of the PCRV and under the service condition the main part of the PCRV are in compression. Due to incressing the loading over the design pressure some parts are cracked and the material behaves nonlinearly. At a loading value of 3.25 times the design pressure the whole transverse section is fully cracked. The total creep curves vs time are gained, the deformations of nodal points after 7 years are 1.8 - 5.5 times larger than those of the initial elastic deformation after the first loading.

For the stage of prestressing, design operating pressure and design limit pressure the vessel behaves elastically. The global safety factory is 1.5 times larger than the design value that shows the conservative design. The analysis method and computer codes which are used in this review, are confirmed afficiently.

+ At present, as a visiting, professor at the Institute of Nuclear Safety Research, KFA, Juelich West Germany, Oct. 1989

DESCRIPTION OF THE PCRV OF A HTR500-TYPE AND ITS ANALYSIS MODEL

The PCRV of a HTR500-type with basaltic concrete was designed by HRB in view of an enhancement of safety and economic aspects (Elter, C. et al 1984). This is conceived in a large-cavity design exactly as that of the THTR300. The core is arranged in the center of the PCRV surrounded by eight heat exchangers. In addition, the PCRV is equipped with penetrations for 72 incore and 48 reflector rods, inspection penetrations and refuelling pipes on the top cap, 3 fuel element discharge pipes at the bottom cap, instrumentation and drains, inspection accesses as well as feed water and main steam connection.

The prestressing system consists of a circumferential and vertical part. The circumferential prestressing is effected using wires of 3/8 inches in diameter. The prestressing wires are placed in prefabricated reinforced concrete parts equipped with sheet-lined channels. The vertical prestressing is using simple conventional linear tendons.

In this calculation an axisymmetric structural model is used. The finite element mesh is show in Fig. 1, for which the maximum nodal point number is 1463 and the maximum element number is 482. Three different types of elements are used in this model, these are 290 quadrilateral, 96 triangular and 96 membrane shell elements.

The operational pressure of this PCRV is 55 bars. The design pressure is 58 bars, which is 1.05 times of the operational pressure.

The size of the vessel,

inner height	17.00m
inner diameter	18.00m
outer height	32.00m
outer diameter	26.50m
thickness of top plate	7.60m
thickness of bottom plate	6.60m
thickness of wall	4.24m

The basic material behaviour,

Concrete:	Young's modulus	$E = 4\ 10^{10}\ N/M^2$
	Poisson's ratio	$\mu = 0.3$
	Uniaxial compressive strength	$f_{cu} = 74.0\ 10^6\ N/M^2$
	Uniaxial tensile strength	$f_{tr} = 3.50\ 10^6\ N/M^2$
Steel:	Young's modulus	$E = 1.96\ 11^{11}\ N/M^2$
	Poisson's ratio	$\mu = 0.3$
	Yield strength (liner)	$\sigma_s = 258.0\ 10^6\ N/M^2$
	Yield strength (Prestressing)	$\sigma_s = 420.0\ 10^6\ N/M^2$

THE HYGROTHERMAL DIFFUSION ANALYSIS

The hygrothermal diffusion analysis consists of the temperature distribution and moisture migration analysis, and these two processes are coupled.

The coupled hygrothermal processes lead to rate equations for heat and moisture balance which are interdependent. Spatial parameterization via finite elements yields a set of coupled first order differential equations which control the evolution of nodel temperature T(t) and relative humidity H(t). (Argyris, J. H., et al 1978)

$$C_T\dot{T} + K_T T = R_T - L_T H - M_T\dot{H}$$
$$C_H\dot{H} + K_H H = R_H - L_H T - M_H\dot{T}$$

where H(t) humidity, and when H=1 corresponds to initial state of full saturation. C_T, C_H capacity matrices describe the heat and moisture storage, separately. K_T, K_H conductivity matrices model heat flow and moisture migration for the driving forces R_T, R_H, separately. The coupling matrices L and M introduce driving forces in the balance equation due to gradients and transients of the other field variables.

The stress-strain response of concrete at elevated temperature is very complex. It depends not only on the material composition, the construction method, the age of concrete etc., but also on the state of humidity. In order to simplify the concomitant identification problem which requires very complex testing, the assumption of weak coupling between the two fields is taken, in the sense that only drying is affected by the temperature field, but thermal transport evolves indepently of the moisture field.

So, take the assuming of $L_T = M_T = 0$, such that above forumlas simplify to

$$C_T\dot{T} + K_T T = R_T$$
$$C_H\dot{H} + K_H H = R_H - L_H T - M_H\dot{T}$$

In the temperature range $20^\circ C \leqslant T \leqslant 70^\circ C$ the thermal properties of concrete do not exhibit a strong temperature dependence. Therefore the heat conduction analysis is carried out linearly. In contrast, the hygrothermal diffusion process is highly nonlinear, since the diffusivity of a porous medium depends strongly on the humidity concentration. Moreover, the hygrothermal diffusion properties are also nonlinear in coupling the thermal field and the humidity field.

The vessel is exposed to the environmental effects due to shrinkage and a temperature gradient. The relative humidity and temperature at the inner side, as the initial environmental condition, are 100% and 40°C, and the temperature gradient is 30°C, it is reached within 7 days. While at the outer side they remain on 60% and 40°C, separately. The main results are as following.

1. The temperature value at each nodal point increases linearly vs time up to its own maximum value, and then keep constant in the remaining time. The temperature distribution across the sections of walls and slabs has emerged in a set of smooth curves. It means that the humidity has no influence on the distribution of the temperature. This phenomenon is the inevitable outcome of the above assumption.
2. The distribution of humidity is dependend on time, temperature and the surrounding conditions. Fig. 2 shows the distributions for 4 nodal points at the middle section of the cylinder, the nodal points of the middle part of the cylinder wall are in the similar case as the sealed specimen, so they have a smaller change. But the other two show a bigger change, especially for the points on the outside of the vessel, e. g. No. 716. The Fig. 3 shows the distribution of the middle section of the cylinder at different days as mentioned above at the outside the environmental condition influence the moisture migration seriously.

THE CREEP ANALYSIS

Creep is the slow increase of deformation due to sustained load, and shrinkage is a stress independent long time deformation, caused mostly by drying. In concrete creep deformation exceeds typically several times the instantaneous elastic deformation and shrinkage is typically of similar magnitude as the elastic deformation.

In this analysis the rate of creep method and a power law is used for parameterization of the rate equation. In the summation model for concrete creep the inelastic response behaviour is described by three deformation components, an aging instantaneous contribution, an aging flow component and a non-aging delayed elastic after effect. This creep model provides ample flexibility to approximate concrete creep data as a function of load duration, age of loading as well as temperature and humidity. The above creep model is essentially linear in stress and exhibits ageing, temperature and moisture dependence in the individual deformation components of the total strain.

For the creep analysis we take the viscoelastic rate formulation into incremental form with forcing term for environmental loading.

$$KD = R_P + R_T + R_H + R_I$$

where K is the elastic stiffness, D is the deformation, R_P is the increment of mechanical loading, R_T is the increment of temperatural loading, R_H is the increment of humidity loading and R_I is the initial load increment due to inelastic behaviour.

This calculation of creep behaviour is carried out up to 7 years (2555 days) using the model of SEKI and KAWASUMI. In this model, the loss of prestressing forces, the influences of temperature, humidity and the interaction between them are fully considered. As mentioned before in the following calculation the weakly coupled of interaction between temperature and humidity to creep is postulated. It means the temperature gradients and temperature transients affect the drying processes, while the heat flow mechamism is not influenced by the moisture field. Up to the end of the 3rd year the total value of loss of prestressing forces is 10%, and then it decreases slowly up to the end of the 40th year. At that time the total loss of prestressing forces reaches 20% (Altes, J. 1984). The loading case is show in Fig. 4. Fig. 4-1 shows the mechanical loading, after 128 days the vessel is prestressed. From the 494th day to the 730th day it is loaded, after this unloaded, and 100 days later reloaded again. Fig. 4-2 shows the environmental loading. Outside the vessel, the surrounding relative humidity is 60%. At the 131th day, heating started from 40°C up to 70°C in 7 days, it means after the 137th day the vessel reaches a steady thermal situation.

1. The contours of deformations
   The contours of deformations are shown in Fig. 5, from these the more vivid concept of creep deformation is given, Fig. 5-1 shows the situation at the 137th day, just reaching the steady thermal state and 9 days after prestressing. Due to thermal creep the deformations are more developed. Fig. 5-2 shows the 495th day, one day after loading, 1 year after prestressing. Owing to the creep effects the deformations of the contour of vessel are fully developed.
2. The total creep curves vs time are given in Fig. 6. Fig. 6-1 shows the creep curves of nodal points 697 and 716, which are located at the inner and outer side of the middle section of the cylinder wall. Fig. 6.2 and Fig. 6-3 show the creep curves of the middle nodal points of the top and bottom slabs. In these figures the total procedure of creep deformations is shown. The nodal point No. 716 for example, gets a radial decrease of 4.3mm after prestressing. One year later as a result of thermal creep an additional radial value of 10.4mm appears and the total deformation reaches 14.7mm. After loading an increase of 3.21mm occurs and under the concerned efforts of prestressing forces, loading and thermal creep up to the 730th day, the deformation decreases 2.4mm. At the 730th day unloading begins. At the 830th day unloading is finished and at that time the radial deformation gets a value of -1.5mm. This value is near to the value of -1.47mm before the first loading, it is 0.03mm higher due to the effects of creep. At the end of the 7th year the total loss of the prestressed forces is increased to 13.2% of the value after reloading. There are similar phenomena for other nodal

points, e. g. for the middle nodal point of the top slab, the total axial deformation after 7 years is 5.5 times of the initial elastic deformation after the first loading. For the middle nodal point of the bottom slab, the total axial deformation after 7 years is 1.8 times of the initial elastic deformation after the first loading.

3. The variation of stresses
The variation of the stresses is more complex than that of the deformations. Taking nodal point No. 716 as an example, after prestressing $\sigma_x = -0.60 \ 10^7 \ N/M^2$, this is a decrease of about 10%. After 7 years the stress value shows some increase but remains nearly the same. The variation of the stress of nodal point No. 571 shows some differences. Compared with the value of the reloading case the value of 7 years has emerged a decrease about of 4%. But for the nodal point No. 1434 it is quite different. At the end of the 7th year it increased about 187%. So, in general, owing to the effects of creep the stresses decreased. But in some places the stresses increased due to redistribution and even the sign of the stresses might be changed.

THE CRACKING AND ULTIMATE LOAD ANALYSIS

The tensile weakness of concrete and the ensuing cracking that results therefrom is a major factor contributing to the nonlinear behavior of reinforced concrete elements. The tangent modulus approach (variable moduli) provides a simpler model for simulating the degradation of stiffness according to the theory of hypo-elasticity. The three parameters failure surface is used. The Mohr-Coulomb criterion with tension cut-off is used for predicing material failure in the form of cracking or sliding due to excessive tension and shear. In the case of cracking the excess tensile stress is redistributed to the surrounding via initial loads. For the Mohr-Coulomb type of failure with two potential sliding planes the stress redistribution technique should be treated according to different failure cases (Argyris, J. H. , et al 1976). In the calculation the intermediate transfer strategy assumes that the centroid of Mohr's circle remains fixed.

The criteria of judgement of the vessel failure can be summarized as followings (Bangash, Y., 1982):

- Computed concrete strength exceeding the available concrete strength under complex loads, cracking and smashing are appeared in the concrete sections; plastic hinges-cum-cracks or penetrating cracks are formed; the entire structure turns to as a mechanism.
- Computed rupturing strength exceeding the minimum experimental rupturing strength of the tendons.
- Limiting crack sizes affecting the integrity of the vessel.
- Yielding or plasticity of the liner crossing a crack.
- Reaching the condition of ultimate equilibrium.

This cracking and ultimate load analysis is carried out up to 178.75 bars (3.25 times the operating pressure). In order to be more suitable for this calculation the finite element mesh has been refined, and the additional membrane shell elements are used to simulate the effects of the prestressing tendons in the cylindrical part. In addition, in some local high tensile stress areas appropriate reinforcements have to be arranged to improve the capability of anti-cracking. The main results are as the followings:

1. Owing to the high concentrated stresses the first cracks appeared at the support area at the loading of 6.875 bars. Accompanied with the raising of loading cracks occured at the inner corner at the pressure of 48.125 bars which is 0.875 times of the operating pressure. At the operating pressure of 55 bars the cracks at the inner corner are more developed, as shown in Fig. 7. But there are no

more cracks except these at the inner corner and the support area.

2. The first cracks at the bottom plate appeared at 1.375 times the operating pressure because of the influence of the penetrations. At a loading of 1.75 times of the operating pressure the middle part of the cylinder and the top plate start to crack in the radial direction.
3. At the design ultimate loading (2.25 times the operating pressure) the cracks are fully developed as shown in Fig. 8. The whole section of the middle part of the cylinder is fully cracked some of the cracks are in the radial direction and others are in the normal direction. So there are no penetrating cracks in the section. Even at the design limit loading case the vessel still could be used.
4. Fig. 9 shows the cracking pattern of the section at the pressure of 178.75 bars (3.25 times operating pressure). It indicates the whole procedure of forming the plastic hinges system and the corresponding mechanism.
5. Fig. 10 shows the curve of displacements vs loading cases for the nodal points at the middle of cylinder wall. Down the 16th loading case (2.5 times operating pressure) the curve almost still keeps straight, and after this starts to incline. This phenomenon indicates that the elastic stage is finished and the plastic stage started.
6. At the loading of 3.25 times the operating pressure the vessel is fully cracked, and the plastic hinges are being formed. There are two at the middle of each plate and three at the cylinder wall. It could be seen that the ultimate load of this vessel is about 3.25 times the operating pressure. In other words the global safety factor of this vessel is 3.25 related to the operating pressure of 55 bars. This is 1.5 times higher then the design global safety factor of 2.25. This also indicates that the design of this vessel is conservative.

DISCUSSION

A. Influence of different creep laws

The two different creep laws and three conditions are used to compare the results of some typical cases. They are:

- SEKI-KAWASUMI model (Seki, S., et al 1970)
  - With considering of the influence of humidity on creep(DB scheme)
  - Without considering of the influence of humidity on creep(DC sch.)
- WYLFA concrete creep model (Browne, R. D., et al 1969)
  - Without considering of the influence of humidity on creep(DD sch.)

It means scheme DD and DC have the same creep law but different conditions. While scheme DC and DD have the same condition but different creep laws.

Emphasis is laid on the comparison between the results from these methods with special interest on the middle sections of wall and slabs.

The main results are as followings:

A1. The displacements

A1.1. It has been found that the results of DB and DC are almost similar and near together. The results of DB are a little bit higher than the results of DC (For example, at point No. 716 after one year the difference is 0.77%).

A1.2. It has been found that different creep laws give quite different speeds. For example, at the 65th day (17.8% days of one year) scheme DD has 90% of the deformations of one year, while

DB only gives 65% of the deformations of one year and after the 165th day (45% of one year) it reached 90% of the deformations of one year (Fig. 10).

A1.3. At the end of one year the deformation of DB is 4.0 - 4.4 times of DDs'.

A2. Stresses

The difference of stresses (e. g. σ_x) between these three schemes are more distinctly.

A2.1. It has been found that the differences between schemes DD and DC are quite larger and in the most cases the stresses of scheme DD are less than the DCs' from 10.0% to 140.0%, but at the same points (e. g. at point No. 571) they increased to about 89.0%.

A2.2. From the speed of decrements it has been found that the speeds are quite different resulting from different creep laws. For the DC scheme it has almost the same value, it means that the influence of creep for this point is very small. But for the DD scheme it is faster and at the end of one year it decreased to 89.0%.

A2.3. The DB scheme just has shown the influence of humidity. Owing to the existence of humidity the decrements of σ_x at point No. 716 are faster.

A2.4. At the inner side of the PCRV the decreasing gradient of humidity is less than that at the outer side. So, at these points the variation of stresses is less than that at the outer side.

B. Influence of temperature on the creep behaviour

The effect of temperature on creep of concrete is a complicated phenomenon. But factors affecting creep have the same influence at elevated temperatures and at room temperature. These factors include time under load, applied stress, maturity of concrete and moisture content of concrete etc. Here are only the comparison of calculated results between the creep at elevated temperature (thermal creep) and room temperature (room creep).

B1. In general the influence of temperature on creep is positive. After one year's heating, and after 3 years' loading at most parts of the vessel the deformations increase, only at some parts they decrease.

B2. After three years the relevant increase of thermal creep to room creep is from 130.7% - 239.5%. It means owing to the elevated temperature $\Delta = 30^{\circ}C$ the creep deformations are developed faster. But at some local areas, due to the complicated structure in some periods the opposite situation could be found.

B3. The relevant increased deformations are listed in the following.

From 128th day to 137th day, at the end of this period the temperature is constant. The ratio of thermal creep to room creep is from 97.3% to 197.1%.

From 137th day to 493th day (the day just before loading), in this period only temperature is existing. The ratio of thermal creep to room creep is from 96.5% to 318.2%. The influence of temperature is apparent gradually.

From 493th day to 730th day, this is the period of first loading. There are comprehensive efforts of creep and loading. The ratio of thermal creep to room creep is from 151.7% to 162.9%, the average value is 1.5 times.

From 730th day to 830th day, this is the period of unloading, and only the efforts of creep are existing. The ratio of thermal creep to room creep is from 141.9% to 156.9%, the average is 1.5 times.

From 830th day to 1095th day, this is the period of reloading. Again

there are comprehensive efforts of creep and loading. The ratio of thermal creep to room creep is from 146.8% to 158.6%, the average value is 1.5 times.
From 128th day to 493th day, this is the period in one year without loading. The ratio of thermal creep to room creep is from 96.74% to 276.97%.

So, the following conclusions would be believed warranted.
- The temperature efforts to creep are positive, but due to the complicated structure at some parts the oppositive efforts are found.
- In general, the results of thermal creep are 1.5 times larger than those of room creep.

CONCLUSIONS

1. In the prestressing stage most parts of the vertical section of the PCRV are under compression stresses which are less than the permissible value. Only in the support area and the inner corner area occur tension stresses and some of them exceed the permissible value, at these places reinforcements are needed.

2. In the case of service conditions most parts of the PCRV still remain in compression. But the tension stresses at the corners (including both the inner and outer corner) are higher, most of them exceed the permissible value. These area has to be reinforced with rebars.

3. In order to get more details of the stress levels for some sensitive areas, especially for the corner and penetration areas, a three dimensional analysis is needed.

4. The creep deformations (in most parts of the PCRV) exceed the elastic deformations in this calculation up to the end of the 7th year, 1.8 - 7 times. The variations of the stresses are more complex, in some areas also the sign changes.

5. The most typical deleterious effect of creep and shrinkage in structures is cracking, both invisible microcracking and, at a later stage, continuous visible cracks. So a cracking analysis especially taking account of the influence of creep is needed.

6. The analysis of creep effects is further complicated by moisture migration as well as simultaneous thermal changes. The moisture effects are much more involved and much less understood than the effects analyzed so far. So, suitable experimental data are needed to carry out a more accurate analysis.

7. The first cracks appeared at the inner corners at the pressure of 48.13 bars, which is 0.875 times of the operating pressure. The first cracks at the bottom plate appeared at 1.375 of the operating pressure. At the design ultimate loading (2.25 times the operating pressure) the cracks are fully developed, but the whole vessel still can be used.

8. At the loading of 3.25 times the operating pressure the vessel is fully cracked, and plastic hings are formed. It could be considered that the ultimate load of this vessel is 178.75 bars. The vessel is designed conservatively enough.

ACKNOWLEDGEMENT

The authors would like to express their deepest gratitude to Prof. J. Eibl and Prof. K. Willam for their many valuable discussions and comments. Special acknowledgement is also directed to DI. J. Szimmat, DI. G. Faust and Dr. H. S. Mueller for their kind proposals of many improvements in this calculation and many valuable discussions and to Dr. Becker and Dr. Weber for handing over of design documents.

Sincere thanks are also directed to Mr. Koschmieder, DI. Beckers and DI. W. Voelzer for their kind help in this calculation.

REFERENCES

Argyris, J. H., Szimmat, J. and Willam, K. J., Inelastic Finite Element Analysis of Massive Concrete Structures, ISD report No.215, Stuttgart, Feb. 1978.

Argyris, J. H., Szimmat, J., et al, SMART Manual, ISD University Stuttgart, Germany, 1982.

Altes, J., et al, Spannbetonbehaelter unter Hypothetischen Stoerfallbelastungen. Foerderungsvorhaben RS 447, KFA Juelich, Jan. 1984.

Bangash, Y., Cracking Analysis of Prestressed Concrete Reactor Vessels, Gas Cooled Reactors Today, BNES, London 1982, pp. 161-166.

Browne, R. D., Blundell, R., The Influence of Loading Age and Temperature on the Long Term Creep Behaviour of Concrete in a Sealed, Moisture Stable State. Extrait de Materiaux et Constructions Vol. 2, 1969.

Elter, C., Becker, G. and Weber, A., The HTR500 Prestressed Concrete Reactor Vessel, Specialists Meeting on Vessel Concepts for Gas-cooled Reactors. Lausanne, Switzerland, Dec. 4-7, 1984.

Koschmieder, D. and Altes, J., RAPS-Ein Dreidimensionales Plotprogramm zum Test und zur Ergebnisdarstellung von Finite Element Berechnungen. Juel - 1596, Juelich, Aug. 1980.

Seki, S. and Kawasumi, M., Creep of Concrete at Elevated Temperatures, Proc. Concrete in Nuclear Reactors, Berlin 1970, ACISP 34 Detroit 1972, pp. 591 - 638.

Wang, T. J. and Altes, J., Stress Analysis and Review of a Prestressed Concrete Reactor Pressure Vessel of a HTR500-TYPE, KFA Juelich, West Germany, 1988.

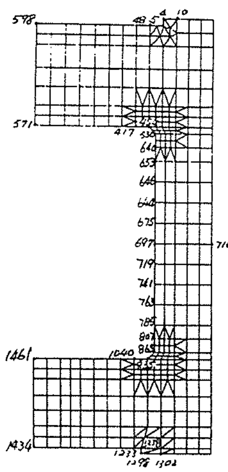

Fig. 1 Mesh of model

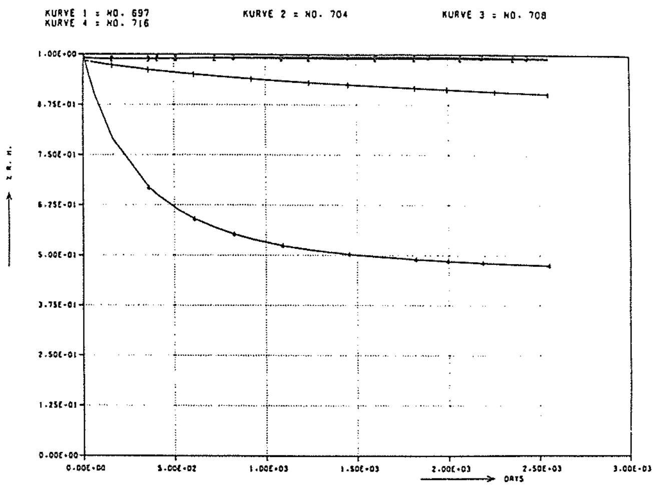

Fig. 2 The humidity value at some nodal points

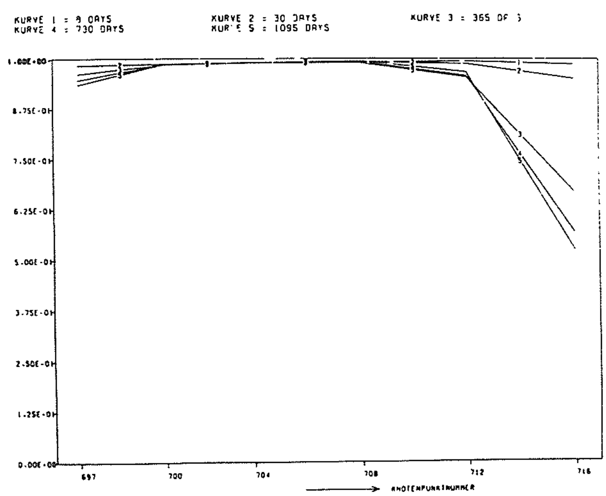

Fig. 3 The humidity distribution at the middle section of cylinder

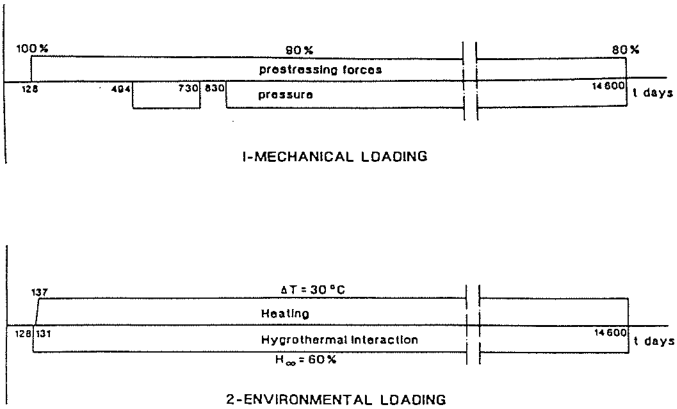

Fig. 4 The loading cases

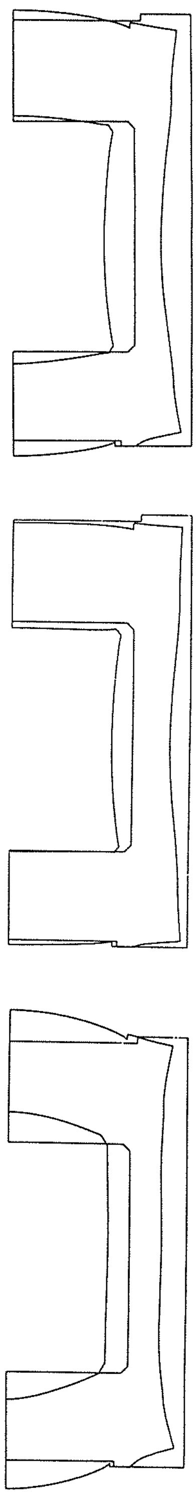

Fig.5 The contours of deformations

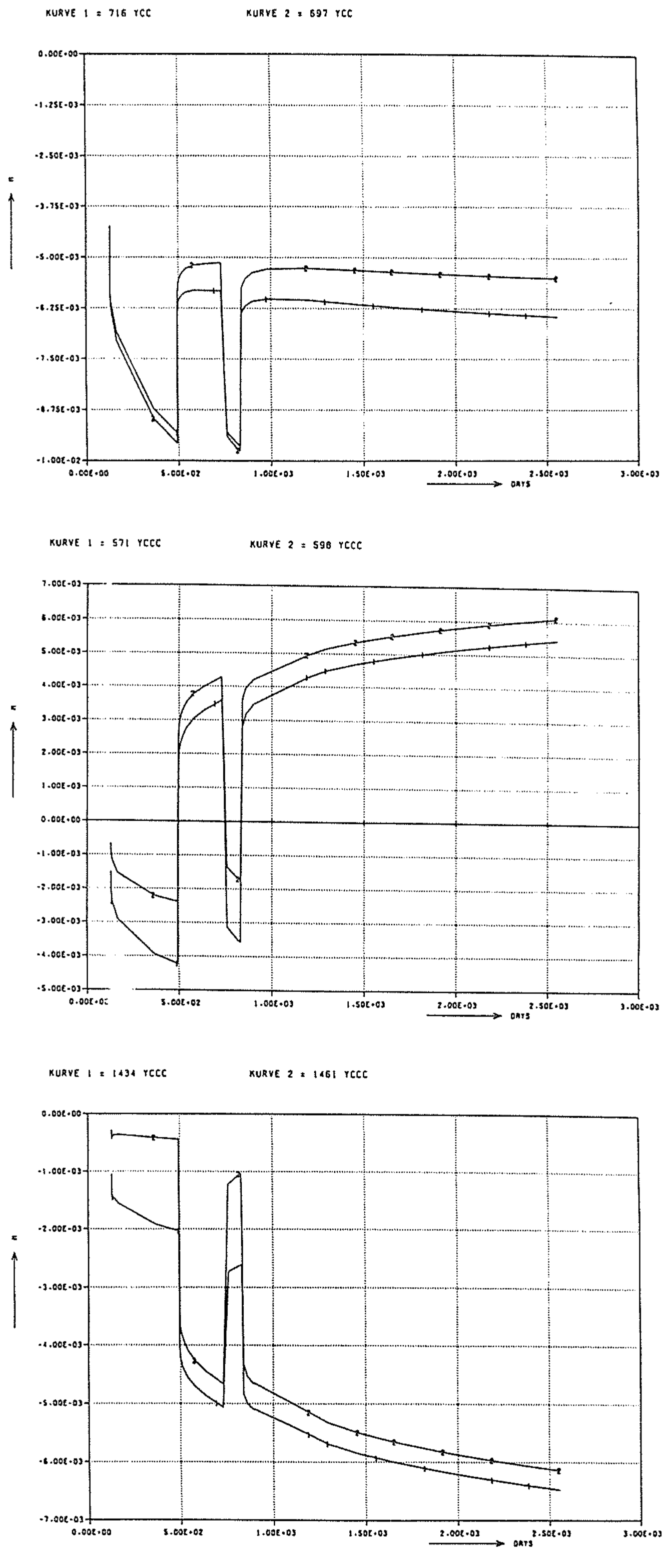

Fig.6 The creep curves

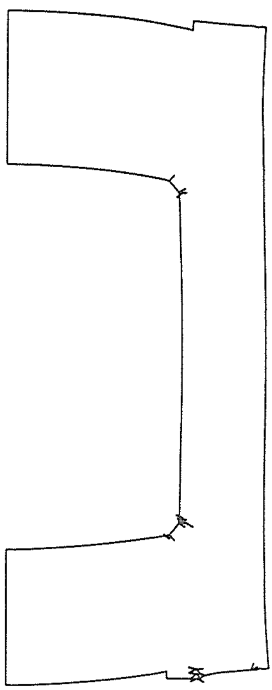

Fig. 7 The cracking and deformation at 55.00 bars

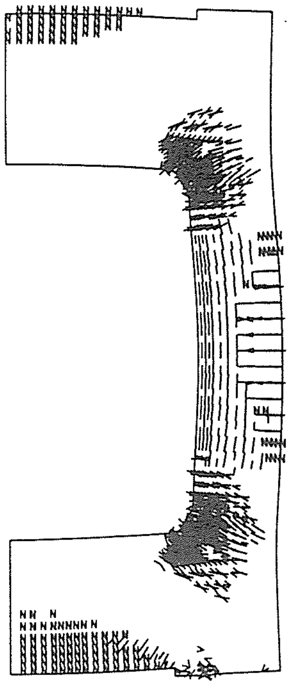

Fig. 8 The cracking and deformation at 123.75 bars

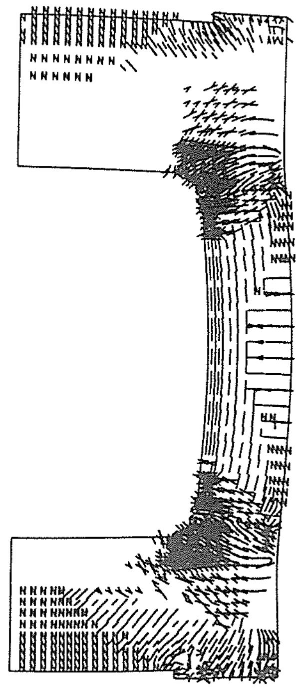

Fig. 9 The cracking and deformation at 178.75 bars

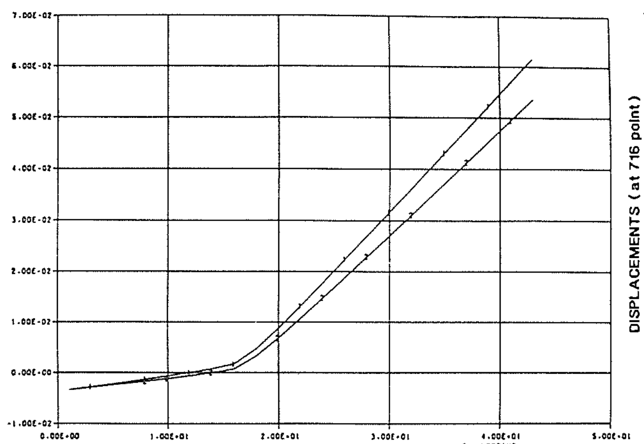

Fig. 10 Displacements vs loading cases at points 697(upper) and 716(below)

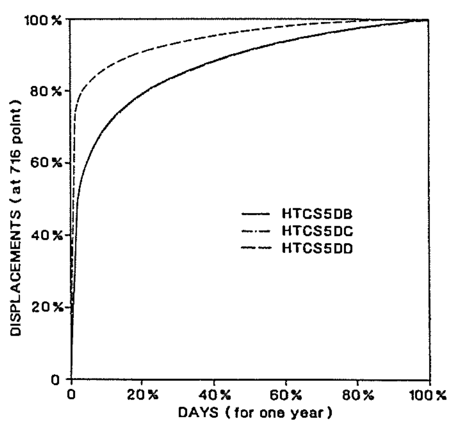

Fig. 11 The comparison of deformations between schemes